communications earth & environment

Article

A Nature Portfolio journal

https://doi.org/10.1038/s43247-025-02268-3

Fluids from deep subducted sediments control the seismic behavior of the Lesser Antilles megathrust

Yaocen Pan[1,2] ✉, Nathalie Feuillet[2], Cecile Prigent[2], Hélène Carton[2], Lianjun Li[3] & Christian Hübscher[4]

At subduction zones, downgoing topographic features exert first-order structural and hydrologic effect on the plate boundary and the upper plate. Such process has been rarely documented by clear observations, especially at great depths, and it remains elusive how the altered structural and physical characteristics of the upper plate control seismogenic behavior and tectonic evolution of margins. Here, we present a reprocessed multichannel seismic (MCS) profile together with bathymetry and earthquake data in the central Lesser Antilles. A reflector imaged at 15-18 km depth ahead of the Tiburon ridge delimits the base of inner forearc crust with pervasive reflective anomalies. It is interpreted to represent a shallow fluid-rich decollement warped over the rough topography, where the underlying materials consist largely of oceanic sediments identical to those accreted at the Barbados prism and basement fragments from basal erosion. Our results suggest that fluids are expelled upward from the band of subducted sediments, leading to a NW-SE elongated zone of hydrofractured and weakened crust above a serpentinized mantle corner coinciding with a prominent aseismic corridor. The high interplate seismic activity offshore Martinique at ~30–65 km depths may correspond to deeply subducted indurated sediments that act as a strong asperity on the plate interface.

Subduction of seamounts and submarine ridges exerts a strong control on forearc hydrology and stress state, and megathrust mechanical and seismogenic behaviors[1–7]. In contrast to the model of subducting seamounts generating strong asperities[4], a more widely held view is that they induce complex fault and fracture networks and a heterogeneous stress field in the upper plate, thereby decreasing the plate coupling[3,8]. In the North Hikurangi subduction zone, seamounts and surrounding fluid-rich sediments are suggested to cause shallow Slow Slip Events (SSE) at <10 km depth[6,9,10]. A large number of studies have also revealed that seamount indentation can lead to severe deformation and damage in the overriding plate, strong heterogeneity in forearc pore fluid pressure and tectonic erosion at the plate interface[1,6,11–16]. Due to the lack of direct observations, the links between seamount subduction, forearc tectonics, interplate processes, and fluid circulation are not well understood, in particular where these topographic features are being subducted at depth beneath the mantle wedge.

In the Lesser Antilles, a series of submarine ridges located on the North and South American plates, parallel and adjacent to Atlantic oceanic fracture zones, subduct obliquely beneath the Caribbean plate at ~18–20 mm/yr in an N67° direction[17]. The two main subducting ridges on the northern Lesser Antilles are the Barracuda and Tiburon ridges, with heights reaching ~2 km (Fig. 1a). They are unbuoyant oceanic-basement ridges, interpreted as having been uplifted during the post-Miocene convergence between the North American and South American plates along pre-existing structural weaknesses, and as a consequence of the oceanic lithosphere deformation along transform faults of the Mid-Atlantic ridge[18,19]. At the southern leading flank of the Tiburon ridge (150 km long and ~40 km wide outboard of the trench), trench-filled sediments are over 3 km thick[20,21], composed of pelagic, volcanoclastic deposits, and terrigenous input from South American rivers. Accretion of the latter since the Eocene has resulted in the world's widest accretionary prism (i.e., the Barbados accretionary wedge) up to 280 km wide and 20 km thick.

Subducting ridges are thought to have a first-order influence on along-strike segmentation and tectonic evolution of the Lesser Antilles subduction zone[22,23]. Although still debated, the process of ridge subduction has been suggested to be responsible for the westward shift of the arc volcanoes north of 15°N since ~10 Ma[23–25]. Moreover, previous seismic imaging revealed a

[1]Department of Earth Sciences, Uppsala University, Uppsala, Sweden. [2]Institut de Physique du Globe de Paris, Université de Paris Cité, CNRS, Paris, France. [3]Department of Earth Science and Engineering, Imperial College London, London, UK. [4]Institute of Geophysics, University of Hamburg, Hamburg, Germany. ✉e-mail: yaocen.pan@geo.uu.se

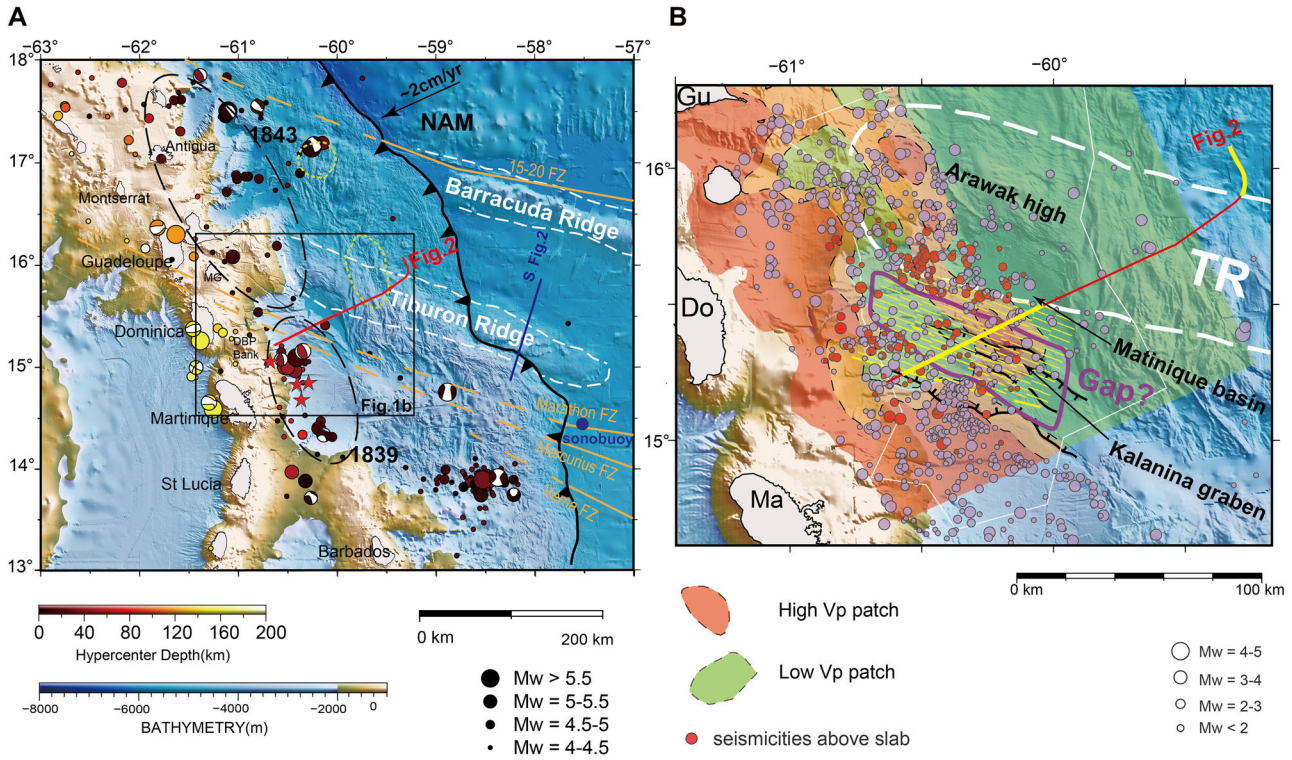

Fig. 1 | Maps of the research area. a Bathymetric map, tectonic setting and seismic survey of the study area in the northern-central Lesser Antilles. The Tiburon and Barracuda ridges subduct obliquely beneath the forearc shown by white dashed lines. The red line indicates the multi-channel seismic profile. The blue line indicates the profile perpendicular to the Tiburon ridge outboard of the trench[20]. The blue point shows the location of the estimate for the thickness of the incoming sediment[21]. All earthquakes shown are > 4 between the years 2014 and 2019, location data from the Institut de Physique du Globe de Paris (IPGP) Data Center, and available focal mechanisms from the Global Centroid Moment Tensor (Global CMT) catalog. Red stars large events 1839, 1946, and 1953. Ellipses the estimated rupture from large historic megathrust events in 1843 and 1839. **b** Bathymetric map superposed by the Vp structure of the slab modified from ref. 39, Vp >7.5 km/s in red, Vp <7.5 km/s in green. Relocated hypocenters from the OBSAntilles survey (survey area outlined by thin white line)[62] are marked by purple dots, red dots indicating events in the overriding plate. Yellow segments of the MCS profile indicate the sediments in the plate boundary revealed in this study. Area with yellow dashed lines indicates the inferred underthrust sediments in front of the Tiburon ridge in this study. M. basin Martinique basin, K. graben Kalanina graben.

few basement highs in the subducting plate beneath the accretionary wedge where oceanic ridges are being subducted[22]. These highs seem correlated with active deformation and fracturing of the above forearc backstop crust and sediments[22,26,27]. Two clusters of seismicity are observed at the intersection of the subducting Barracuda and Tiburon ridges with the backstop[22,28] (Fig. 1b). Seismic reflection data has also revealed that a layer of incoming sediments as thick as 1 km is located below a decollement layer and is underthrust with little deformation below the accretionary wedge, forearc basement, and maybe to deeper levels[26,27]. The thickness of sediments trapped under the decollement varies along strike due to the presence of the subducting ridges, and the largest thickness has been imaged on the southern flank of the Barracuda ridge[22].

Existing multichannel active-source seismic (MCS) surveys and related studies have been mostly carried out at the latitude of the Guadeloupe Archipelago and farther north. Sparse seismological data are recorded from distant land stations, and ocean bottom seismometer (OBS) cruises were of short durations. They are insufficient to reveal the geometry of the plate interface where the Tiburon ridge is subducted beneath the inner forearc. The crucial question of whether the sediments subducted deeper remains unsolved.

Here, we present an integrated interpretation of marine multichannel seismic reflection image, tomographic velocity structures, bathymetry, and earthquake data offshore Dominica-Martinique, which reveals the structural and hydrological processes in the upper plate and interplate fault in response to subduction of the Tiburon ridge with a high spatial resolution at depth. Our work points to anomalous sediments and ascending fluids at the leading flank of the Tiburon ridge that leads to hydrofracturing in the arc basement and hydration in the mantle wedge corner. The newly documented complex nature of the plate interface in the Lesser Antilles likely plays a key role on controlling the spatial variability of the inter-plate coupling.

Results and discussion

Seismic reflection image

We reprocessed (see method section) and re-examined a MCS profile shot using an 8865 in ref. 3 airgun source during the SISMANTILLES-2 cruise of R/V L'Atalante in 2007[29]. The MCS profile is over 180 km long in the forearc and transects the underthrust Tiburon ridge (Fig. 1a for location). For the entire section (i.e., Fig. 2a), we performed Kirchhoff post-stack time migration using a root-mean-square (RMS) velocity converted from the wide-angle velocity model[30] (Supplementary Fig. 1). For the inner forearc domain (i.e., Fig. 3a), to better resolve the intra-basement features, we performed Kirchhoff post-stack time migration using a manually adjusted and smoothed version of the RMS velocity model. The time-depth conversion was based on the wide-angle velocity model[30]. A pre-stack depth migration (PSDM) was also performed in this inner forearc domain (Supplementary Fig. 5).

A distinct low-frequency reflector, R1, previously observed only in the outer domain of the accretionary wedge[31], can be traced arcward to the inner forearc beneath the Martinique Basin, at a distance of 160 km from the trench (Fig. 2b, blue arrows). This reflector, above the multiple, is continuous in the frontal domain and becomes less continuous with a lower-frequency character farther arcward. In general, it shows a rugose morphology with two prominent reliefs; a topographic low of this reflector is seen in the middle at a distance of ~85–100 km from the trench. High amplitude and thicker reflections occur primarily at the seaward/arcward

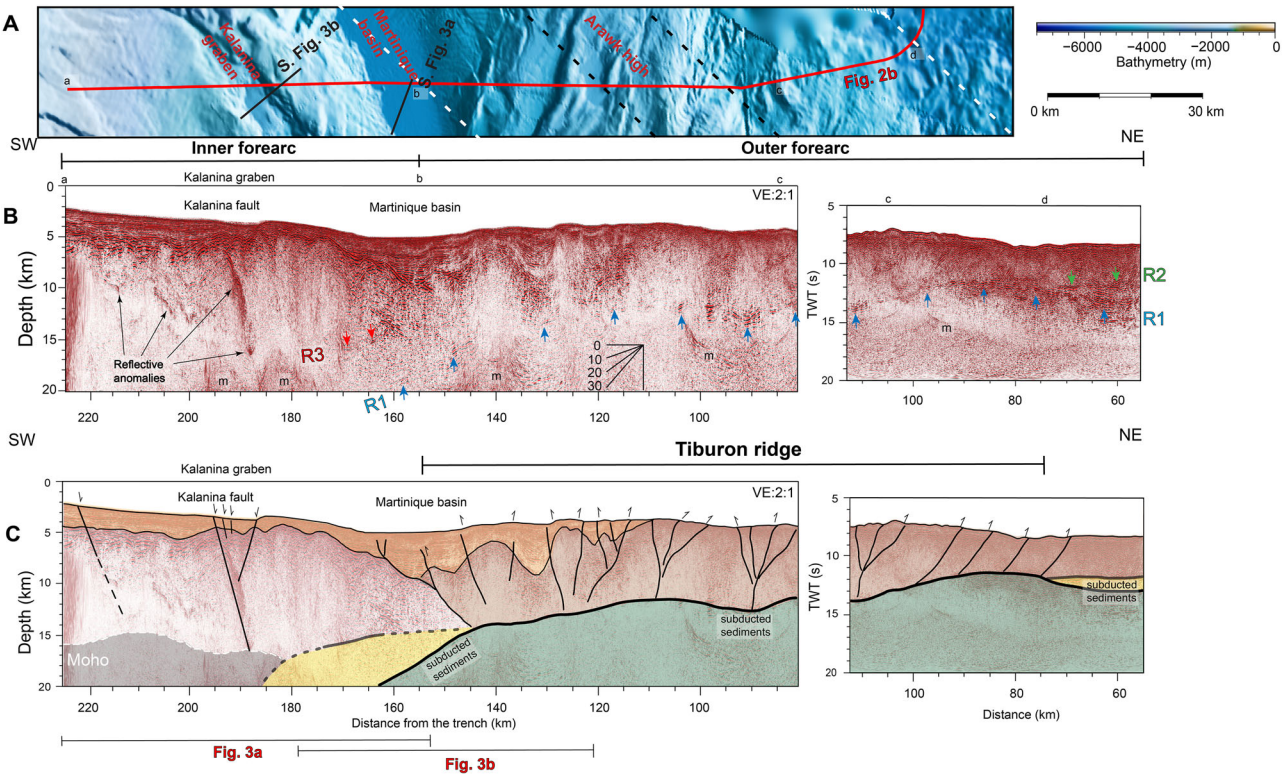

Fig. 2 | Bathymetric and seismic structures along the MCS profile. Bathymetric (**a**), time-migrated and depth-converted reflection image (**b**) with interpretation (**c**) of the MCS profile. While dashed lines indicate the extent of the underthrust Tiburon ridge. Black dashed lines indicate the Arawk high coincides with the peak of the inner relief. Blue arrows point to reflector R1, green R2, and red R3. Moho is modified from ref. 39. M denotes the multiple.

ends of this reflector and this topographic low, whereas high-frequency and weaker reflectivity tends to occur at the topographic highs. At the eastward end of the profile, we observed that a reflector, R2 (Fig. 2b, green arrows), lies above the R1 and is absent arcward of 70 km.

In the inner domain from a distance of 160 km to 220 km, for the first time we observe pervasive reflection amplitude anomalies with negative polarity relative to the seafloor reflection (Fig. 3 and Supplementary Fig. 4, 5). The Kalanina fault is the major fault bounding the northern Kalanina graben to the southwest. The sedimentary strata show a normal sense of displacement at this fault (Fig. 3b). Prominent reflection amplitude anomalies, found at a distance of 190 km down to a depth of 16 km, are in alignment with the trace of the Kalanina fault at the seafloor. Other reflective anomalies appear to also correlate spatially to normal faults in the overlying sediment cover.

Beneath the Martinique basin, an arcward-dipping reflector (R3, Figs. 2, 3, Supplementary Figs. 4, 5) is newly observed from a distance of 165 km to 173 km, ~4–5 km above the reflector R1. R3 is located at a depth varying from 14 km to 16 km and displays a dip of ~8°, shallower than the underlying R1 (dip of ~15°). R3 appears as a moderate-to-high-frequency, discontinuous reflector (Fig. 3a). It shows negative polarity at a distance of 165 km at ~15 km depth (Fig. 3a insert 3, Supplementary Figs. 4, 6, 7). At a distance of 170 km, the R3 becomes a suite of stacked reflectors with an overall thickness greater than 1 km (Fig. 3a insert 4). Deeply penetrative normal faults beneath the forearc slope terminate at this reflector (Fig. 3b). The region above R3 has an overall high reflection amplitude. By contrast, the underlying domain exhibits a broad arcward-gently-dipping reflective zone of low amplitude and diffused and chaotic facies.

Structure of the subduction interface and forearc domain

We interpret that the reflector R1 originates from the top of the descending Atlantic oceanic crust and that the two prominent reliefs of ~2 km height delimit the extent of the subducting Tiburon ridge beneath the accretionary wedge (Fig. 2c). A seismic profile perpendicular to the Tiburon ridge east of the trench highlights that this ridge has an irregular morphology with multiple kilometer-scale sub-ridges of oceanic crustal rocks with troughs in between filled by marine sediments[20] (Supplementary Fig. 2; location of the profile on Fig. 1a). In our profile, oblique to the Tiburon ridge, the topography of the R1 reflector agrees well with such geometry, thus indicating that the morphology of the ridge has been preserved when entering subduction.

According to previous studies[26,27], we interpret the reflector R2 in the most trenchward position as the decollement formed in a lower Miocene unit rich in smectitic clay, which separates the upper accreted and lower underthrust sediments. R1 shows a well-stratified pattern at about 140–150 km distance from the trench (Fig. 2), indicating the presence of intact subducted sediments at the leading flank of the Tiburon ridge. Similar well-stratified reflectors are visible above the reflector R1 at 85–100 km distance, indicating that lower plate sediments are present in lows between sub-ridges.

Above the subducting Tiburon ridge, backthrusts and thrusts developed in the accretionary wedge. Compressional deformation in the upper plate above a subducting relief is compatible with observations from other subduction zones and results from analog and numerical models[13,32]. The imbricate thrusts and backthrusts are seen rooted at the reflector R1 (Figs. 2, 3d), indicating that reflector R1 acts as an active slip surface in the updip direction.

In the west inner forearc, the Tiburon ridge is in contact with the forearc crust of the upper plate that acts as a backstop (Fig. 2c). Numerous normal faults crosscut the upper plate, suggesting an extensional regime in this forearc domain (Fig. 3b) as also observed in Guadeloupe[33,34].

Origin of the R3 and implication for underthrust sediments

Below the inner forearc crust, our results indicate the presence of another reflector, reflector R3, above the subducting plate (Figs. 2, 3), at a depth of 14–18 km. This vertical-incidence reflector identified in the MCS profile coincides with a wide-angle reflector identified in wide-angle reflection/

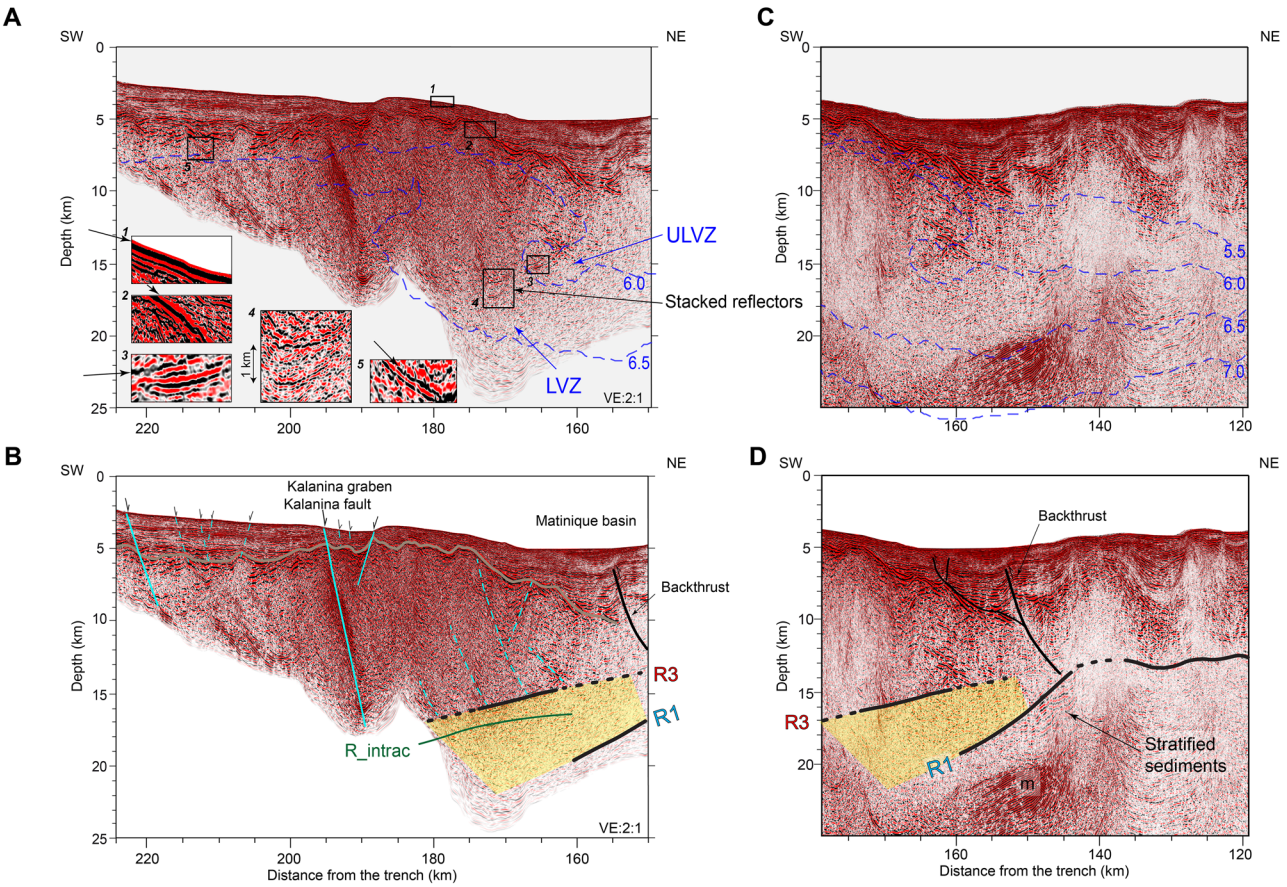

Fig. 3 | Selected inner portions of the MCS profile. a selected portion of the MCS profile in the inner forearc domain reveals abundant reflective amplitude anomalies in the inner forearc. Small boxes show notable reflections with reversed polarities (3,5) with respect to the normal polarities of the seafloor (1) and basement top (2). Note that the first coherent event (arrowed) in subset 3 and 5 is black, not red. **b** Interpretation of the image. Green line indicates the reflector inverted from OBS-recorded PicP phase. Light blue lines indicate fluids-charged fault and fractures, which are apparently connected to the R3. **c** Selected portion of the MCS profile at the transition between inner and outer forearc. **d** Interpretation of the image. Yellow areas correspond to the inferred interlayered sediments. See text for further details. Blue dashed lines show Vp contours of 5.5 − 7.0 km/s[30]. M denotes the multiple.

refraction data[30] within a depth difference of <1 km depth (green reflector in Fig. 3b and Supplementary Fig. 1, see ref. 30). From published cross-sections of the forearc domain, two possible origins for this reflector and the material sandwiched between R3 and R1 could be envisioned. R3 could be either an intra-crustal reflector separating two blocks of fore-arc crust[28,35,36] or the contact between the fore-arc crust and the mantle wedge below[37]. Based on our results and other geophysical observations, we thereafter propose an alternative hypothesis, that the material between R3 and R1 may represent accreted sediments in the leading flank of the Tiburon ridge.

The interpretation of R3 as an intra-crustal structure was based on seismic imaging of a discontinuity at ~28 km depth within the upper plate that was interpreted as the (flat) upper plate Moho[36]. Ductile shearing may occur at around 15 km in the upper plate for accommodating the plate convergence and form mylonites[38], which can be highly reflective in seismic data. At the latitude of Guadeloupe, an intra-basement arcward-dipping thrust fault has been proposed at a depth of 10–15 km resulting from interaction between the backstop and subducted ridges[35,36]. However, more recent studies using gravity and magnetic data[37] and regional seismic tomography[39] suggested a convex-upward upper plate Moho at a shallow depth of 15–20 km. Moreover, the inner forearc crust exhibits extensional permanent deformation, whereas compressional structures in the upper plate do not appear to extend arcward of the backthrust. We have no evidence of an intra-crustal arcward dipping reverse fault. Ref. 37 suggested ~35% of peridotite serpentinization at the shallow depth of 15–30 km in the wedge corner. The reflector R3 may represent a contact between the forearc crust and underlying serpentinites formed during mantle wedge hydration above the megathrust. Such a lithological boundary is commonly characterized by a single reflection with positive polarity, for example, the S-reflector at rifted margins[40], which is, however, inconsistent with R3 observed here with layered reflectors and negative polarity.

Trenchward of the Kalanina fault, the inner forearc is marked by a low velocity zone (<6.5 km/s, Fig. 3a and Supplementary Fig. 1) down to 20 km, which was resolved based on high-resolution OBS tomographic inversion[30]. At a distance of 165 km, we note that R3 is strikingly collocated with an ultra-low velocity zone (ULVZ, P-wave velocities of 5.5–6 km/s, blue arrow on Fig. 3a). High reflectivity and low-velocity zones are ubiquitous in subduction zones, interpreted as either overpressured oceanic crust beneath a low-permeability seal at the plate interface[41,42], or fluid signatures at the plate interface, in many cases, enriched in sediments[10,43]. Here, the top of the oceanic crust, R1, lies clearly more than 4–5 km beneath the ULVZ (Figs. 2b, 3c, d), suggesting that the former is unlikely.

The observation of a high-frequency R3 reflector at 165 km, together with the small dimension of the ULVZ, would imply that fluids are trapped at a rather thin interface that may be overpressured. Further downdip at 170 km, the layered reflectors indicate that R3 consists of multiple interfaces. The contrasts of reflectivity across R3 cannot be caused by insufficient penetration of the airgun-source, because the strong reflection from R1 is seen at a depth up to 18 km (Figs. 2, 3c). Instead, this contrast should imply a lithological change and/or fluid content variation. The underlying materials of weaker reflectivity would have a lower fluid content than that at R3 and, further above, in the fractured crust. This interpretation agrees with the Vp/Vs structure showing a decrease from 1.8-1.84 to 1.78-1.8 in

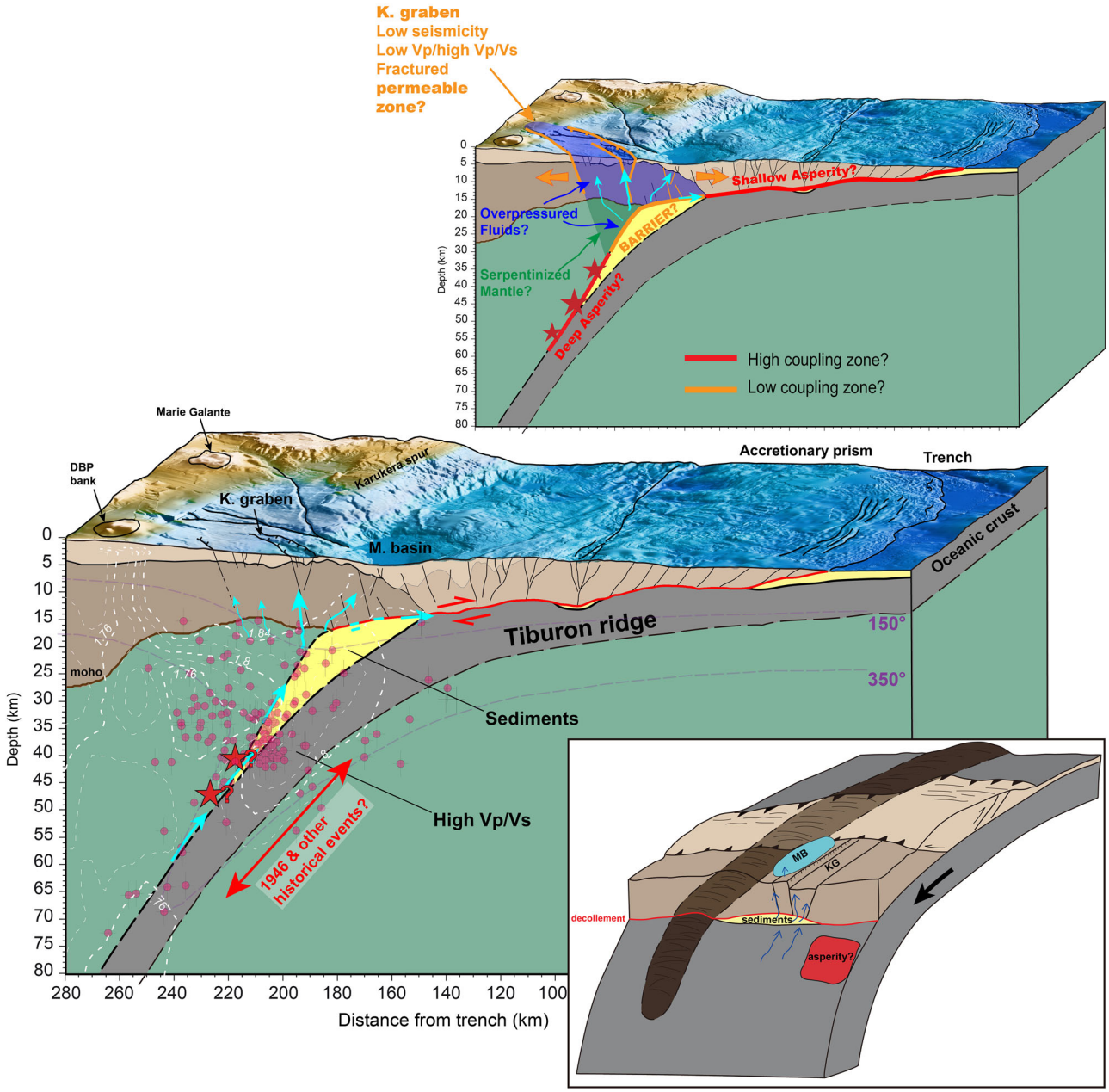

Fig. 4 | Interpreted block diagram of the Tiburon ridge subducting beneath the Central Lesser Antilles. Perspective view shows bathymetry, geometry of the plate boundary, and structures and fluids signature in the upper plate. Tomographic Vp/Vs and Moho are from ref. 39. Seismicities selected from ref. 62 have uncertainty of 1.5 km in epicenter and 2.5 km in depth, and are within 20 km laterally of our profile. The 150 °C and 350 °C isotherms are from ref. 56. Lower right insert: schematic model of the fluid flow and damage in the upper plate in response to the Tiburon ridge and subducted sediments.

the underlying materials at the immediate downdip edge of the Tiburon ridge (Fig. 4, ref. 39).

In the northern Hikurangi margin, unusually large volumes of sediments were found associated with underthrust seamounts, where fluid concentration peaks at the crestline of the underthrusting sediments[9]. The topographic features can result in a step-up of the decollement when subducted[15]. We infer that a wide zone of sediments originating from the sediment-rich incoming Atlantic seafloor may exist downdip of the Tiburon ridge, composing largely the materials between reflectors R1 and the R3. This material could also include ancient prismatic materials entrained in the subduction and crustal fragments removed due to basal erosion[44]. We believe that R3 represents a shallow fluid-bearing decollement that lies at the contact between the overriding crust and the interlayered sediments. Although the R3 reflector is less clear downdip, where there is blanking and a vertical pattern of the reflections, we observe that the shearing is localized upon the interlayered sediments (Figs. 2, 3). This suggests that the sediments can be transported to greater depths.

In the northern Hikurangi margin, the sediments were largely accreted in the mantle up to 40 km depth due to high resistance for further subduction[45]. In the Lesser Antilles, sediment subduction driven by the Tiburon ridge would have begun since the ridge started subducting in the early Miocene[24]. Their present-day accumulation in the offshore Dominica-Martinique sector would have contributed to a compositional and chemical heterogeneity within the mantle corner[31]. Such locality is evidenced by a thickened Wadati-Benioff zone[46] and a dominant stress of downdip compression at intermediate depths thought to be related to resistant slab materials piled in the mantle[47]. Geochemical signatures of lavas from the active Martinique arc suggest a sediment-rich input[48].

Various independent observations revealed an along-strike discontinuity (e.g., low velocity) of the slab near 15N[49–51]. These observations are consistent with our model, where the presence of an anomalously large volume of sediments would exert a strong influence on the hydration and stress state of the slab. One would expect, for instance, delayed metamorphic reactions of the downdip hydrous minerals, as excess sediments usually transport additional fluids into the mantle, cooling the slab. Such an effect may also contribute to the relatively insulated forearc mantle and the primary fluids release and melts in the subarc and backarc[52].

Evidence for fluid flow through the upper plate and their potential source

In the outer forearc accretionary wedge, local strong reflective zones in both upper and plate interface may represent fluid-saturated regions, associated with the low degree of consolidation in the forearc[53] and high clay content at the plate interface[54]. In the inner forearc crust, we suggest that the pervasive intra-basement reflective zones are due to the presence of aqueous fluids because the trapped fluids have much lower impedance than the host rocks above, which can cause strong reflections with negative polarity. Our interpretation is supported by the overall high Vp/Vs > 1.8 in this region[39] (Fig. 4), indicating that the forearc basement hosts a substantial amount of fluids. Shallow high-resolution seismic and chirp data show large acoustic blanking zones that are likely fluid escapes within the uppermost sedimentary unit in areas of the Martinique basin and Kalanina graben (Supplementary Fig. 3).

Sediment compaction and drainage of free pore fluid from sediments and slab crust are thought to take place within the upper 10 km depth of the interplate fault[55]. It thus cannot explain the imaged fluid signatures in the inner forearc domain (Figs. 2, 3). In the cold Lesser Antilles subduction zone, dehydration of smectite, abundant in subducted sediments[54], which is estimated to occur at ~150 °C, should take place at ~20 km depth in the mantle wedge[56], underneath our resolved fluid signals in the basement (Fig. 4). Thus, the inferred sediments probably serve as a substantial source for overpressured pore fluids on the plate interface up to ~20 km.

Fluids circulating through the forearc could also originate from deeper metamorphic reactions in the slab, i.e., progressive breakdown of hydrous phases in the subducting crust and mantle (e.g., serpentine, chlorite, amphibole), with released fluids channelized along the subduction interface. Recent studies suggested that the subducting Atlantic lithosphere is highly altered from tectonic and fluid-rock interaction processes on the Mid-Atlantic Ridge axis[57] and on transform faults[51,58], as well as on bending faults at the outer rise[59]. Seismic tomography results suggest that dehydration of the hydrous slab crust and mantle occurs at depths of ~70 km and ~120 km[60]. Along the strike of the subduction, higher seismicity and lower seismic velocities have been evidenced where fracture zones are being subducted, suggesting higher alteration of the lithosphere along these inactive parts of oceanic transform faults[58,60]. The Marathon fracture zone is located beneath the Kalanina graben (Fig. 1). At ~30–60 km depth, mantle wedge earthquakes are largely clustered above the slab and were ascribed to free fluids-induced brittle failure[31,61]. They are, hence, probably triggered by fluid-saturated metasedimentary rocks in the mantle. Beneath Guadeloupe, the presence of a low-velocity layer, documented to be ~15-20 km thick and extending to ~45 km depth[31], also supports this interpretation.

Implications for fluid transport, forearc structures, and the seismogenic behavior of the megathrust

Our data suggest that the rugose subducted oceanic crust is overlaid by subducted sediments lying in front of the Tiburon ridge. The decollement (highlighted in red, Fig. 4) is resolved to ~18 km depth at the distance of ~180 km inboard of the trench, indicating a shallow dip of ~5° of the megathrust at shallow level. High precision earthquake location from the OBSAntilles experiment[62] shows that the dip of the plate interface increases sharply to ~30° downdip. This notable kink in the subduction interface occurs at the intersection with the Kalanina fault (Fig. 4).

Spatially, it is very likely that the underthrust sediments are continuous along the southern flank of the Tiburon ridge (yellow dashed lines, Fig. 1b). It is striking that this area downdip of the Tiburon ridge corresponds to a NW-SE trending corridor of relatively low spatial density of seismicity. This corridor coincides with a band of low Vp (Fig. 1b) and high Vp/Vs at the plate interface[39]. These anomalies were interpreted as a fractured and water-rich zone near which overpressured pore fluids accumulate above the slab. Fluids may originate from hydrated ultramafic rocks near subducting fracture zones or from water-saturated metasediments[39]. This fits well with our observations. The densely fractured Kalanina graben, bounded by the main NW-SE striking Kalanina faults, is likely a permeable zone that acts as a drainage system ahead of the Tiburon ridge above dehydrating subducted sediments (Figs. 1b, 4). Several mantle earthquakes lying below the Kalanina fault (Fig. 4), together with the lateral change in P-wave velocities (~6.0–6.5 km/s) across it (Supplementary Fig. 1), suggest that it serves as a main rheological boundary in the overriding plate, being a main vertical fluid conduit. A magnetic high and gravity low interpreted as caused by the presence of serpentinized mantle[37,63] was documented aligned with the corridor and the low seismic activity region. This is probably related to fluid infiltration above the sediments. Alternatively, the serpentinized forearc mantle could be due to volatiles derived directly from the slab crust and mantle. However, tomographic results suggest small fluxes of the volatiles in a relatively dry and cold mantle wedge, and they largely remain as free fluids discharged in the mantle corner[52]. South of the aseismic corridor, seismic activity is distributed in a region of high velocity at the interface, at around latitude 15°N (Fig.1b). Here, the most prominent cluster of intraplate earthquakes ranges from 30 km to 65 km depth[64]. It may be where large historical events have occurred, e.g., 1839, 1946 (>M 7.0)[65,66]. This locality is over 100 km south of the subducted Tiburon ridge.

Variability in seismic activity along the plate interface thus appears to be in part related to the subduction of the Tiburon ridge and downdip subducting sediments that likely induce strong heterogeneities in the geometry, pore pressure, and frictional properties along the megathrust. Excess mass and buoyancy associated with the ridge could lead to an increased normal stress at the interface and hence enhanced coupling[4] on the shallow part of the megathrust. High fluid pressure above the subducting sediments may have reduced the effective stress at the plate boundary, leading to stable slip regimes and eventually slow-slip or various aseismic events[6,67,68]. No slow-slip event has yet been reported in the Lesser Antilles, however. Along the deeper portion of the megathrust, the underthrust sediments could be overconsolidated, making the area downdip of the ridge prone to earthquake nucleation[1].

Variations in the mechanical properties of the megathrust and the wedge may impart further control on the upper plate structures and the style of faulting[69]. Normal faulting in the upper plate was inferred to result from a high amount of repeated coseismic slip along the shallower part of the megathrust[69]. It may thus be an indicator of repeated updip propagation of earthquakes. A similar seismogenic dynamics could be an explanation for the presence of the Kalinana fault system. Bending of the subduction interface may have also contributed to localizing this main fault, as a result of slip partitioning of motion along a ramp-flat geometry.

Our study reveals that a fluid-rich forearc is associated with subduction of 4–5 km thick sediments driven by the subduction of the Tiburon ridge. The ridge-induced hydrological and structural effects are found to contribute to a lack of seismicity and possibly a velocity-strengthening frictional behavior on the megathrust segment located immediately ahead of the Tiburon ridge. This zone may act as a barrier to rupture propagation. In contrast, there is increased interplate seismic activity further downdip and south of the corridor, where indurated sediments could be located, forming possibly large coherent asperities. The presence of the above barrier may explain why historical ruptures and instrumental earthquakes are confined below the Moho[65,66]. Extensional structures and high pore pressure are commonly documented in other subduction zones that experienced devastating tsunamis[69,70]. In the Lesser Antilles, we cannot exclude, in both the prehistorical times[25] and the future, the occurrence of massive megathrust events at the deep seismic active segment (e.g., offshore Martinique),

similar to the 2011 Tohoku-Oki tsunamigenic earthquake that ruptured across interface structural and frictional heterogeneities and into the shallow domain[71]. In northern Japan, before the Tohoku Oki 2011 earthquake, smaller earthquakes occurred along the deep portion of the plate interface below the Moho[72]. Repeated ruptures of these deeper asperities contributed to loading the shallower part of the megathrust. These processes may also apply to the Lesser Antilles. Our results highlight the need for future experimental observations targeted at the offshore domain for understanding of fluid dynamics and the risk associated with the megathrust seismogenic slip in the Lesser Antilles.

Methods

Multichannel seismic (MCS) reflection data

The deep seismic reflection profile was acquired during the Sismantilles 2 experiment. For details of the acquisition parameters, see ref. 22. The shallow seismic profiles were acquired during CASEIS survey[73] with vessel R/V *Pourquoi pas?*.

The SISMANTILLES-2 profile was originally processed on board up to post-stack time migration with constant velocity (water velocity: 1500 m/s) using CGG-Veritas Geovecteur R and Geocluster R softwares[31]. Our reprocessing of this profile was conducted with Echos and Geodepth software packages from Paradigm Geophysical. The processing flow starts from resampling of the raw shot gathers from 2 ms to 4 ms with a recording length of up to 25 s. The dominant frequency range is 8–25 Hz. After a nominal 2D geometry applied, we adopted bandpass filtering (3–6–32–35 Hz), band-limited swell noise suppression (3–8 Hz). For turn noise mitigation, we used the LIFT method[74]. Then, a predictive deconvolution and a spherical divergence correction were performed. To remove multiples, we used a combination of Radon multiple removal and 2D surface-related multiple removal technique. Velocity analysis was conducted at every 160th common middle point (1 km), followed by normal moveout corrections, stacking, and Kirchhoff post-stack time migration. A time-varying bandpass filter was applied for display. The coincident OBS wide-angle seismic data were collected during the Sismantilles experiment[30]. We used the interval velocity model derived from travel-time tomographic OBS model for converting the time-migrated section into depth domain.

We manually adjusted and smoothed version of the RMS velocity model derived from tomographic velocity model and updated velocity in the time domain at every 80th common middle point (0.5 km). We performed Kirchhoff post-stack time migration using this new RMS velocity model for the inner portion of the MCS profile (Fig. 3a and Supplementary Figs. 4, 6). The structural geometry and dipping features in the basement are better resolved compared to the post-stack time migration image using OBS tomographic model. A Kirchhoff pre-stack depth migration algorithm (Eikonal) was applied to the selected inner portion of MCS profile (Supplementary Fig. 5), using the interval velocity model derived from the OBS tomographic velocity model. Final visualization of data in amplitude scale was performed using HIS Kingdom suite software.

Bathymetry data

High-resolution bathymetric data were acquired with a Resen 7150 multibeam sounder during CASEIS 2016 survey with vessel R/V *Pourquoi pas?*. It was processed using the Caraibes software® (Ifremer) and filtered to produce a DEM with a resolution of 50 m. The shipboard bathymetric data were then merged with data from previous cruises downloaded on GMRT Map Tool, data from the CARAMBA and ANTIPLAC cruises, and a DEM from Ifremer.

Data availability

All geophysical data of the SISMANTILLES and CASEIS cruises are available on the SISMER Database (https://campagnes.flotteoceanographique.fr).

Code availability

Processing of the seismic data has been conducted with Echos and Geodepth software packages from Paradigm Geophysical. Processing of the bathymetric data have been conducted with the Caraibes software® (Ifremer). Adobe Illustrator and GMT were used during all figure preparation.

Received: 28 August 2024; Accepted: 1 April 2025;
Published online: 17 April 2025

References

1. Sun, T., Saffer, D. & Ellis, S. Mechanical and hydrological effects of seamount subduction on megathrust stress and slip. *Nat. Geosci.* **13**, 249–255 (2020).
2. Ruh, J. B., Valentí, S., Ranero, C. R. & Gerya, T. Crustal deformation dynamics and stress evolution during seamount subduction: High-resolution 3-D numerical modeling. *J. Geophys. Res. Solid Earth* 3782–3803 https://doi.org/10.1002/2016JB013250.Received (2016).
3. Wang, K. & Bilek, S. L. Invited review paper: fault creep caused by subduction of rough seafloor relief. *Tectonophysics* **610**, 1–24 https://doi.org/10.1016/j.tecto.2013.11.024 (2014).
4. Small, C. & Scholz, C. H. The effect of seamount subduction on seismic coupling. *Geology* **25**, 487–490 (1997).
5. Singh, S. C. et al. Aseismic zone and earthquake segmentation associated with a deep subducted seamount in Sumatra. *Nat. Geosci.* **4**, 308–311 (2011).
6. Chesley, C., Naif, S., Key, K. & Bassett, D. Fluid-rich subducting topography generates anomalous forearc porosity. *Nature* **595**, 255–260 (2021).
7. Arai, R. et al. Upper-plate conduits linked to plate boundary that hosts slow earthquakes. *Nat. Commun*. **14**, (2023).
8. van Rijsingen, E. et al. How subduction interface roughness influences the occurrence of large interplate earthquakes. *Geochem. Geophys. Geosyst.* **19**, 2342–2370 (2018).
9. Bell, R. et al. Seismic reflection character of the Hikurangi subduction interface, New Zealand, in the region of repeated Gisborne slow slip events. *Geophys. J. Int.* **180**, 34–48 (2010).
10. Bangs, N. L. et al. Subducting seamounts form sediment lenses along the Hikurangi margin and enhance slow slip. *Nat. Geosci*. https://doi.org/10.1038/s41561-023-01186-3 (2023).
11. Ranero, C. R. & Von Huene, R. Subduction erosion along the Middle America convergent margin. *Nature* **404**, 748–752 (2000).
12. von Huene, R. & Scholl, D. W. Observations at convergent margins concerning sediment subduction, subduction erosion, and the growth of continental crust. *Rev. Geophys.* **29**, 279–316 (1991).
13. Gerya, T. V., Fossati, D., Cantieni, C. & Seward, D. Dynamic effects of aseismic ridge subduction: numerical modelling. *Eur. J. Mineral.* **21**, 649–661 (2009).
14. Martinod, J. et al. Effect of aseismic ridge subduction on slab geometry and overriding plate deformation: Insights from analogue modeling. *Tectonophysics* **588**, 39–55 (2013).
15. Bangs, N. L. B., Gulick, S. P. S. & Shipley, T. H. Seamount subduction erosion in the Nankai Trough and its potential impact on the seismogenic zone. *Geology* **34**, 701–704 (2006).
16. Dominguez, S., Lallemand, S. E., Malavieille, J. & Von Huene, R. Upper plate deformation associated with seamount subduction. *Tectonophysics* **293**, 207–224 (1998).
17. DeMets, C., Gordon, R. G. & Argus, D. F. Geologically current plate motions. *Geophys. J. Int.* **181**, 1–80 (2010).
18. Muller, R. D. & Smith, W. H. F. Deformation of the oceanic crust between the North American and South American plates. *J. Geophys. Res. Solid Earth* **98**, 8275–8291 (1993).
19. Patriat, M. et al. Evidence for Quaternary convergence across the North America-South America plate boundary zone, east of the Lesser Antilles. *Geology* **39**, 979–982 (2011).
20. Pichot, T. et al. The Cenozoic tectonostratigraphic evolution of the Barracuda Ridge and Tiburon Rise, at the western end of the North

America-South America plate boundary zone. *Mar. Geol.* **303–306**, 154–171 (2012).
21. Mauffret, A., Westbrook, G. K., Truchan, M. & Ladd, J. The relief of the oceanic basement and the structure of the front of the accretionary complex in the region of Sites 541, 542, and 543. 49–62 (1984).
22. Laigle, M. et al. Along-arc segmentation and interaction of subducting ridges with the Lesser Antilles Subduction forearc crust revealed by MCS imaging. *Tectonophysics* **603**, 32–54 (2013).
23. Bouysse, P. & Westercamp, D. Subduction of Atlantic aseismic ridges and Late Cenozoic evolution of the Lesser Antilles island arc. *Tectonophysics* **175**, 349–355 (1990).
24. Boucard, M., Marcaillou, B., Lebrun, J. & Laurencin, M. Paleogene basins and Neogene subsidence of the Northern Lesser Antilles Forearc. *Tectonics* 1–33 https://doi.org/10.1029/2020TC006524 (2020).
25. Seibert, C. et al. Sedimentary records in the Lesser Antilles fore-arc basins testify the occurrence of large late Quaternary megathrust earthquakes. *Geochem, Geophys. Geosyst.* https://doi.org/10.1029/2023GC011152 (2024).
26. Westbrook, G. K. Cross section of an accretionary wedge: Barbados Ridge complex. *Geology* **16**, 631–635 (1988).
27. Moore, J. C. et al. Consolidation patterns during initiation and evolution of a plate-boundary decollement zone: northern Barbados accretionary prism. *Geology* **26**, 811–814 (1998).
28. Christeson, G. L., Bangs, N. L. & Shipley, T. H. Deep structure of an island arc backstop, Lesser Antilles subduction zone. *J. Geophys. Res. Solid Earth* **108**, 1–17 (2003).
29. Laigle, M., Lebrun, J. F. & Hirn, A. SISMANTILLES 2 cruise, RV L'Atalante. https://doi.org/10.17600/7010020 (2007).
30. Evain, M. Structure sismique de la zone de subduction des Petites Antilles: implications sur les dimensions de la zone sismog'ene interplaque. *Thesis* 38 https://side.developpement-durable.gouv.fr/HDFR/doc/OAI_6/oai-archimer.ifremer.fr-28335/structure-sismique-de-la-zone-de-subduction-des-petites-antilles-implications-sur-les-dimensions-de- (2011).
31. Laigle, M. et al. Seismic structure and activity of the north-central Lesser Antilles subduction zone from an integrated approach: Similarities with the Tohoku forearc. *Tectonophysics* **603**, 1–20 (2013).
32. Dominguez, S., Malavieille, J. & Lallemand, S. E. Deformation of accretionary wedges in response to seamount subduction- Insights from sandbox experiments the features. *Tectonics* **19**, 182–196 (2000).
33. Feuillet, N., Manighetti, I., Tapponnier, P. & Jacques, E. Arc parallel extension and localization of volcanic complexes in Guadeloupe, Lesser Antilles. *J. Geophys. Res. Solid Earth* **107**, 3–29 (2002).
34. De Min, L. et al. Tectonic and sedimentary architecture of the Karukéra spur: A record of the Lesser Antilles fore-arc deformations since the Neogene. *Mar. Geol.* **363**, 15–37 (2015).
35. Bangs, N. L., Christeson, G. L. & Shipley, T. H. Structure of the Lesser Antilles subduction zone backstop and its role in a large accretionary system. *J. Geophys. Res. Solid Earth* **108**, 2358 (2003).
36. Kopp, H. et al. Deep structure of the central Lesser Antilles Island Arc: Relevance for the formation of continental crust. *Earth Planet. Sci. Lett.* **304**, 121–134 (2011).
37. Gailler, L. et al. Forearc structure in the Lesser Antilles inferred from depth to the Curie temperature and thermo-mechanical simulations. *Tectonophysics* **706–707**, 71–90 (2017).
38. Jones, T. D. & Nur, A. The nature of seismic reflections from deep crustal fault zones. *J. Geophys. Res. Solid Earth* **89**, 3153–3171 (1984).
39. Paulatto, M. et al. Dehydration of subducting slow-spread oceanic lithosphere in the Lesser Antilles. *Nat. Commun.* **8**, 1–11 (2017).
40. Reston, T. J. et al. Movement along a low-angle normal fault: The S reflector west of Spain. *Geochem. Geophys. Geosyst.* **8**, 1–14 (2007).
41. Audet, P., Bostock, M. G., Christensen, N. I. & Peacock, S. M. Seismic evidence for overpressured subducted oceanic crust and megathrust fault sealing. *Nature* **457**, 76–78 (2009).
42. Bostock, M. G. The Moho in subduction zones. *Tectonophysics* **609**, 547–557 (2013).
43. Calvert, A. J., Preston, L. A. & Farahbod, A. M. Sedimentary underplating at the Cascadia mantle-wedge corner revealed by seismic imaging. *Nat. Geosci.* **4**, 545–548 (2011).
44. von Huene, R., Ranero, C. R. & Vannucchi, P. Generic model of subduction erosion. *Geology* **32**, 913–916 (2004).
45. Reyners, M., Eberhart-Phillips, D. & Stuart, G. A three-dimensional image of shallow subduction: Crustal structure of the Raukumara Peninsula, New Zealand. *Geophys. J. Int.* **137**, 873–890 (1999).
46. Bie, L. et al. Along-arc heterogeneity in local seismicity across the Lesser Antilles subduction zone from a dense ocean-bottom seismometer network. *Seismol. Res. Lett.* **91**, 237–247 (2019).
47. Mike, L. Bayesian regional moment tensor from ocean bottom seismograms recorded in the Lesser Antilles: implications for regional stress field. *Geophys. J. Int.* **108**, 1036–1054 (2023).
48. Hu, Y., Teng, F. Z. & Chauvel, C. Potassium isotopic evidence for sedimentary input to the mantle source of Lesser Antilles lavas. *Geochim. Cosmochim. Acta* **295**, 98–111 (2021).
49. Harris, C. W., Miller, M. S. & Porritt, R. W. Tomographic Imaging of Slab Segmentation and Deformation in the Greater Antilles. *Geochemistry, Geophys. Geosystems* **19**, 2292–2307 (2018).
50. Van Benthem, S., Govers, R., Spakman, W. & Wortel, R. Tectonic evolution and mantle structure of the Caribbean. *J. Geophys. Res. Solid Earth* **118**, 3019–3036 (2013).
51. Schlaphorst, D. et al. Water, oceanic fracture zones and the lubrication of subducting plate boundaries-insights from seismicity. *Geophys. J. Int.* **204**, 1405–1420 (2016).
52. Hicks, S. P. et al. Slab to back-arc to arc: Fluid and melt pathways through the mantle wedge beneath the Lesser Antilles. *Sci. Adv*. **9**, 1–33 (2023).
53. Bangs, N. L. B., Westbrook, G. K., Ladd, J. W. & Buhl, P. Seismic velocities from the Barbados Ridge complex: indicators of high pore fluid pressures in an accretionary complex. *J. Geophys. Res. Solid Earth* **95**, 8767–8782 (1990).
54. Moore, J. C. et al. Abnormal fluid pressures and fault-zone dilation in the Barbados accretionary prism: evidence from logging while drilling. *Geology* **23**, 605–608 (1995).
55. Saffer, D. M. & Tobin, H. J. Hydrogeology and mechanics of subduction zone forearcs: fluid flow and pore pressure. *Annu. Rev. Earth Planet. Sci.* **39**, 157–186 (2011).
56. Ezenwaka, K. et al. Thermally-constrained fluid circulation and seismicity in the Lesser Antilles subduction zone. *Earth Planet. Sci. Lett.* **597**, 117823 (2022).
57. Davy, R. G. et al. Wide-angle seismic imaging of two modes of crustal accretion in mature Atlantic Ocean Crust. *J. Geophys. Res. Solid Earth* **125**, 1–21 (2020).
58. Cooper, G. F. et al. Variable water input controls evolution of the Lesser Antilles volcanic arc. *Nature* **582**, 525–529 (2020).
59. Allen, R. W., Collier, J. S. & Henstock, T. J. The role of crustal accretion variations in determining slab hydration at an Atlantic subduction zone. *J. Geophys. Res. Solid Earth* **127**, 1–21 (2022).
60. Bie, L. et al. Imaging slab-transported fluids and their deep dehydration from seismic velocity tomography in the Lesser Antilles subduction zone. *Earth Planet. Sci. Lett.* **586**, 117535 (2022).
61. Halpaap, F. et al. Earthquakes track subduction fluids from slab source to mantle wedge sink. *Sci. Adv*. **5**, eaav7369 (2019).
62. Ruiz, M. et al. Seismic activity offshore Martinique and Dominica islands (Central Lesser Antilles subduction zone) from temporary onshore and offshore seismic networks. *Tectonophysics* **603**, 68–78 (2013).

63. Gailler, L. S. et al. Crustal structure of Guadeloupe islands and the Lesser Antilles arc from a new gravity and magnetic synthesis. *Bull. La Soc. Geol. Fr.* **184**, 77–97 (2013).
64. Corbeau, J. et al. A Significant Increase in Interplate Seismicity near Major Historical Earthquakes Offshore Martinique (FWI). *Bull. Seismol. Soc. Am*. 1–18 https://doi.org/10.1785/0120200377 (2021).
65. Weil-Accardo, J. et al. Two hundred thirty years of relative sea level changes due to climate and megathrust tectonics recorded in coral microatolls of Martinique (French West Indies). *J. Geophys. Res. Solid Earth* **121**, 2873–2903 (2016).
66. Philibosian, B. et al. 20th-century strain accumulation on the Lesser Antilles megathrust based on coral microatolls. *Earth Planet. Sci. Lett.* **579**, 117343 (2022).
67. Kodaira, S. et al. High pore fluid pressure may cause silent slip in the Nankai Trough. *Science.* **304**, 1295–1298 (2004).
68. Warren-Smith, E. et al. Episodic stress and fluid pressure cycling in subducting oceanic crust during slow slip. *Nat. Geosci.* **12**, 475–481 (2019).
69. Cubas, N., Avouac, J. P., Leroy, Y. M. & Pons, A. Low friction along the high slip patch of the 2011 Mw 9.0 Tohoku-Oki earthquake required from the wedge structure and extensional splay faults. *Geophys. Res. Lett.* **40**, 4231–4237 (2013).
70. Tsuji, T. et al. Extension of continental crust by anelastic deformation during the 2011 Tohoku-oki earthquake: The role of extensional faulting in the generation of a great tsunami. *Earth Planet. Sci. Lett.* **364**, 44–58 (2013).
71. Tajima, F., Mori, J. & Kennett, B. L. N. A review of the 2011 Tohoku-Oki earthquake (Mw 9.0): Large-scale rupture across heterogeneous plate coupling. *Tectonophysics* **586**, 15–34 (2013).
72. Uchida, N. & Bürgmann, R. A decade of lessons learned from the 2011 Tohoku-Oki Earthquake. *Rev. Geophys.* **59**, 1–44 (2021).
73. Feuillet, N. CASEIS cruise, RV Pourquoi pas? https://doi.org/10.17600/16001800 (2016).
74. Choo, J., Downton, J. & Dewar, J. LIFT: a new and practical approach to noise and multiple attenuation. *First Break* **22**, 39–44 (2004).

Acknowledgements

We thank the SISMANTILLES scientific party for providing the seismic data. We thank Marie-Paule Bouin for providing the earthquake relocations. We thank the editor Joe Aslin, Derya Gürer, and two anonymous reviewers for their constructive review. Paradigm and IHS Kingdom are thanked for providing academic licenses for seismic processing and interpretation. This work was supported by funding from the French ANR CARQUAKES (contract number ANR17-CE03-0006).

Author contributions

Y.P., N.F., C.P., and H.C. analyzed the MCS data, bathymetric data, tomographic velocity structures, and earthquake data and interpreted the data. H.C. and C.H. supervised the data processing. L.L. contributed to the data processing. Y.P. wrote the first draft of the paper. N.F., C.P., and H.C. reviewed and revised the paper. All authors contributed to scientific discussions.

Funding

Open access funding provided by Uppsala University.

Competing interests

The authors declare no competing interests.

Additional information

Supplementary information The online version contains supplementary material available at https://doi.org/10.1038/s43247-025-02268-3.

Correspondence and requests for materials should be addressed to Yaocen Pan.

Peer review information *Communications Earth & Environment* thanks Lidong Bie and the other, anonymous, reviewer(s) for their contribution to the peer review of this work. Primary Handling Editors: Derya Gürer and Joe Aslin. A peer review file is available.